Paper submitted July 1993

Neural Network Prediction of Aluminum-Lithium Weld Strengths From Acoustic Emission Amplitude Data

by Eric v. K. Hill,* Peggy L. Israel,† and Gregory L. Knotts‡

Abstract

Acoustic emission (AE) flaw growth activity was monitored in aluminum-lithium weld specimens from the onset of tensile loading to failure. Data on actual ultimate strengths together with AE data from the beginning of loading up to 25 percent of the expected ultimate strength were used to train a backpropagation neural network to predict ultimate strengths. Architecturally, the fully interconnected network consisted of an input layer for the AE amplitude data, a hidden layer to accommodate failure mechanism mapping, and an output layer for ultimate strength prediction. The trained network was then applied to the prediction of ultimate strengths in the remaining six specimens. The worst case prediction error was found to be +2.6 percent.

Keywords: acoustic emission, aluminum-lithium, amplitude distribution, backpropagation, failure mechanism, neural network, ultimate strength.

INTRODUCTION

The 2195-T87 aluminum–lithium alloy is being considered as a replacement material for the 2219-T87 aluminum currently in use on the Space Shuttle External Tank. Both materials exhibit good weldability and strength, but the aluminum–lithium is less dense and 25 percent stronger, thereby providing extra payload capacity; hence, the incentive for change. Because variable polarity plasma arc welding is the principal method of joining, and the welds are typically the weakest link (Nunes et al., 1984), weld strength is paramount to external tank structural integrity. A method is developed here for predicting ultimate weld strengths at proof loads as low as 25 percent of the expected ultimate using acoustic emission (AE) data.

The AE data taken during proof loading have been correlated with ultimate strengths in both composites (Kalloo, 1988; Hill, 1992; and Walker, 1992) and in metals (Hill and Knotts, 1993). These correlations used such AE parametric data as amplitude, energy, and event rate to quantify the AE signals generated by the various failure mechanisms. Thus, AE data contain information concerning failure mechanisms which can be correlated to ultimate strengths in engineering materials.

The different characteristics of the AE signals correspond to different deformation and failure mechanisms during loading. For example, rubbing noises (from specimen grips) and plastic deformation generate AE signals that are similar to one another but typically very much different from the AE signals produced by crack growth or intermetallic precipitate fractures (McBride et al., 1981). Since each of these deformation and failure mechanisms contributes in varying degrees to the structural integrity of a finsihed part, in generating an ultimate strength prediction equation, the AE associated with each mechanism must be weighted differently (have a different coefficient). The AE events associated with rubbing and plastic deformation, which contribute little or nothing to the ultimate strength, would have weighting functions (coefficients) approaching zero, while those that contribute significantly, such as crack growth or intermetallic precipitate fractures, would have large coefficients. Neural networks provide an automated technique for sorting out the AE associated with the various mechanisms and determining the appropriate coefficients or weighting functions (Sachse and Grabec, 1992). Therefore, neural networks were employed in this research to generate ultimate strength predictions from the AE amplitude data.

NEURAL NETWORK TRAINING

Acoustic Emission Amplitude Distributions

The acoustic emission amplitude parameter, A [dB], is a logrithmic representation of the peak signal voltage, V [V], of the AE waveform

$$A = 20 \log(V/V_i) \tag{1}$$

For most applications, $V_i = 1$ μV at the sensor output is chosen as the 0 dB reference because it is the lowest detectable voltage, just slightly above the noise level of the system electronics. Here the AE sensor contained a built-in 40 dB preamplifier; consequently, 0 dB was referenced to 100 μV at the preamplified sensor output (Mitchell, 1984).

Acoustic emission amplitude distributions (events vs. amplitude histograms) have been shown to contain information that allow the identification of failure mechanisms in materials (Pollock, 1981). The (differential) amplitude distribution can represent peak signal voltages of the AE waveforms ranging from 100 μV (0 dB) to 10 V (100 dB). The various failure mechanisms are typically seen grouped together as characteristic humps or bands in the amplitude distribution, and while the amplitude bands for such mechanisms as plastic deformation and crack growth are widely separated, there are other mechanisms whose characteristic amplitude bands overlap. This overlap in the AE failure mechanism amplitude bands is accentuated by attenuation effects, especially dispersion (Miller and McIntire, 1987). Here, because the specimens were small, the attenuation effects in the AE waveforms were expected to be minimal. It was therefore hoped that the amplitude distributions would have enough separation in the failure mechanism bands to allow accurate prediction of ultimate strengths in the aluminum–lithium weld specimens.

The amplitude distribution for specimen 01-5 is shown in Fig-

Embry-Riddle Aeronautical University, Aerospace Engineering Dept., 600 S. Clyde Morris Blvd., Daytona Beach, FL 32114; (904) 226-6748.
* Lamar University, Computer Science Dept., Beaumont, TX 77710; (409) 880-8782.
‡ Acoustic Emission Consultants, 13490 Shelly Dr., Madison, AL 35758; (205) 232-8163.

ure 1. Note that there are five distinct humps or AE amplitude (failure mechanism) bands and 307 total AE events. Because the logarithms of measurements tend to have normal distributions (Tennant-Smith, 1985), the various failure mechanism humps in the amplitude distribution were approximated as such. This being the case, the first mechanism probably has amplitudes between 4–12 dB; the second mechanism ranges from approximately 8–20 dB; the third from 19–29 dB; and the fourth from 34–35 dB. The fifth hump is a single event at 91 dB representing specimen failure. It can be seen that there is some overlap between the first and second and the second and third mechanisms; moreover, inasmuch as the first hump does not appear to be normally distributed, there may well be more than one mechanism buried within it (Kouvarakos, 1992). Modeling these humps and determining the effect of the various mechanisms is where neural networks come into play.

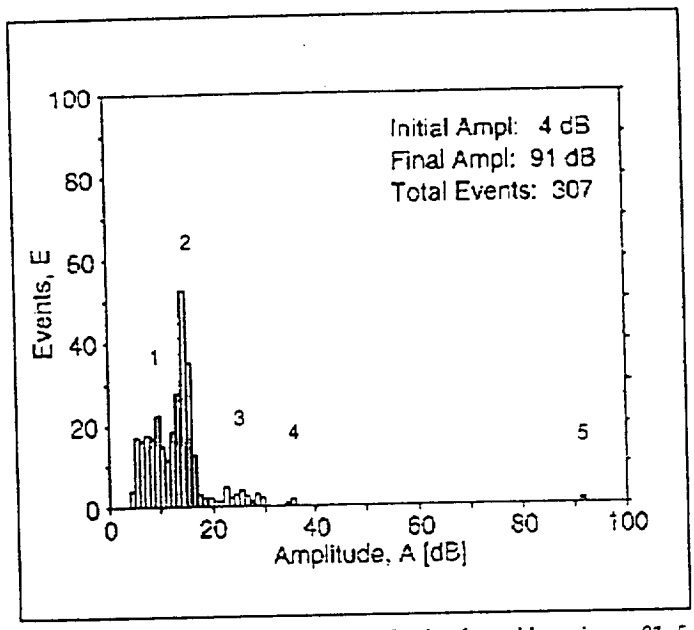

Figure 1—Differential amplitude distribution for weld specimens 01–5.

Neural Networks

The beauty of neural networks lies in the fact that they can take into account the effects of the various failure mechanisms without explicitly identifying and/or isolating them from the rest of the data. Moreover, given the appropriate structure and input, neural networks can learn all the pertinent data interactions and make accurate predictions using the entire data set, regardless of extraneous data (such as AE from rubbing noises) or data overlap and without having to resort to multivariate statistical analysis. These brain-like responses are generated through the use of artificial neurons.

An artificial neuron in its simplest form is shown in Figure 2(a). Here the w_i are the weight vector components, and the x_i are the input vector components. Within the artificial neuron each input vector component is multiplied by its respective weight vector component; then these products are summed up over all the inputs to yield the NET output:

$$\text{NET} = \Sigma_i w_i x_i \tag{2}$$

Such a neuron can be used to model linear processes or provide a linear mapping from the input to the output.

In order to accommodate nonlinear mappings (solve nonlinear problems), a nonlinear activation function, F, must be applied to the NET output as shown in Figure 2(b). The nonlinear activation function employed here is the sigmoid (meaning S-shaped) or squashing function:

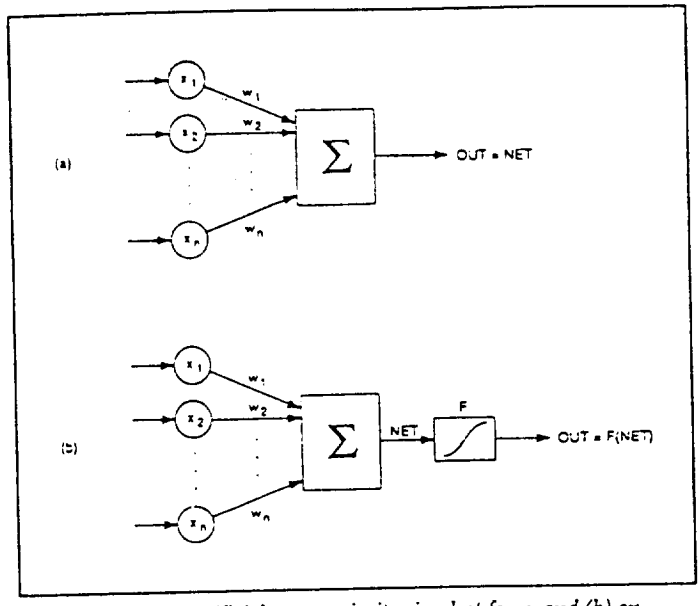

Figure 2—(a) An artificial neuron in its simplest form, and (b) an artificial neuron with a nonlinear activation function.

$$\text{OUT} = F(\text{NET}) = [1/(1 + e^{-\text{NET}})] - 0.5 \tag{3}$$

As the value of NET approaches large negative values, OUT approaches a limiting value of -0.5; when NET is equal to 0, OUT is equal to 0; and as NET grows large in a positive sense, OUT approaches a value of +0.5. Figure 3 is a plot of this function. In addition to allowing the solution of nonlinear problems, the nonlinear gain provided by the sigmoid activation function allows the same neuron to process both very large and very small inputs without noise saturation problems (Wasserman, 1989). This two layer network with multiple inputs and a nonlinear activation function is known as a perceptron.

Many problems cannot be represented by a single nonlinear mapping. For such problems, multiple or nested nonlinear mappings can be obtained by cascading layers of perceptrons together to form multilayer networks. These consist of an input layer, an output layer, and one or more middle or hidden layers. It should be mentioned that multilayer networks provide no increase in computational power over two layer networks unless nonlinear activation functions are included within each layer of neurons (Wasserman, 1989).

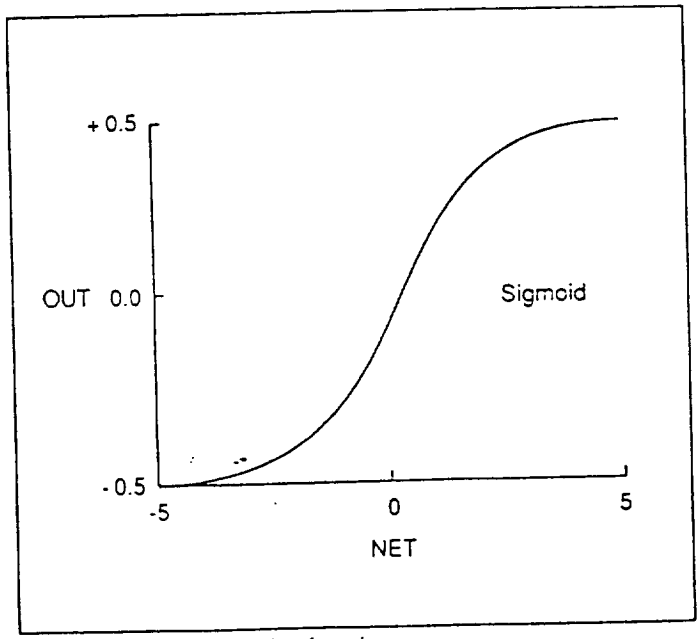

Figure 3—Sigmoid activation function.

From Figure 4 it can be seen that the amplitude histogram, $E(A)$, is an approximation to the actual amplitude distribution, $e(A)$ (Zurada, 1992). Each rectangle in the histogram (Figure 5a) can be modeled by a three layer network consisting of two perceptrons in parallel followed by a single neuron to sum their outputs (Figure 5b). Binary activation functions in the perceptrons are used to create the square corners of the rectangle: one perceptron to map the up-side and one to map the down-side. This binary approximation to the amplitude histogram is designated $E(w_{ij},A)$, where w_{ij} denotes the interconnection weight to neuron i from neuron j. When the binary activation functions are replaced by continuous activation functions, such as the sigmoid, the result becomes a smooth line approximation, $e(w_{ij},A)$, to the actual amplitude distribution, $e(A)$, creating sigmoidal humps instead of rectangles (Figure 5a). Hence, this three layer network provides a nonlinear mapping followed by a linear mapping. More commonly, multilayer networks employ nonlinear activation functions throughout, meaning that each neuron layer produces a nonlinear mapping. Such is the case in this application.

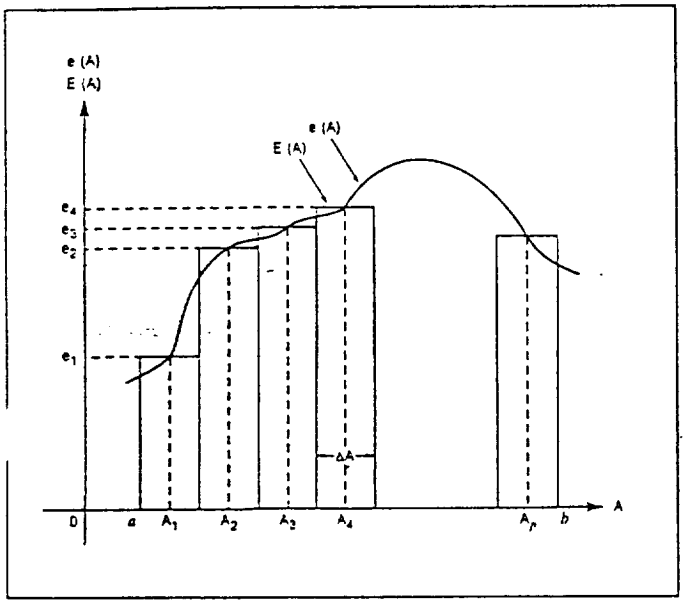

Figure 4—Amplitude histogram.

Training is accomplished by adjusting the interconnection weights such that known input amplitude data produce known ultimate strengths as outputs. This means that inputting the amplitude distribution for specimen 01-5 should yield its ultimate strength of 51.5 ksi (0. 355 kPa) as the output. The known input (amplitude distribution) and target output (ultimate strength) constitute what is called a training pair. When both the input and the output are known, the training is designated supervised learning. Typically, several training pairs (specimens) are needed to train the network and arrive at the appropriate weight components. Once the network is trained, a set of test data is used to verify the prediction accuracy of the neural network. The test data set, like the training set, consists of known inputs with known outputs. Thus, a prediction error can be calculated and network performance assessed.

Backpropagation

Backward error propagation or backpropagation is a training method that compares the actual output of the network with the expected or target output, then backpropagates adjustments in the weights proportional to the calculated error. The object of training is to adjust the weights such that the application of a set of inputs produces the desired or target output. Hence, network training is a two step procedure—forward and backward—propagating the inputs and their concomitant activations forward to the output layer, then propagating the error backward from the output layer through the hidden layer(s) to upgrade the interconnection weights.

For the ANSim software package used herein, a bias neuron is included in every layer except the output layer (Figure 6). Each bias

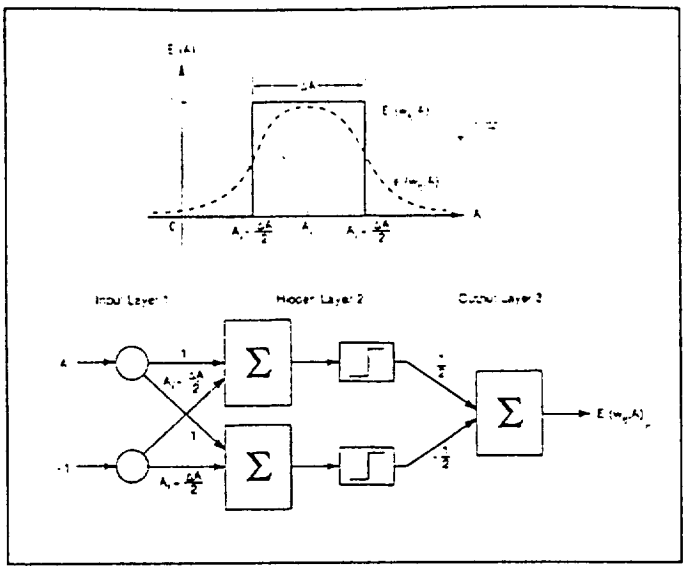

Figure 5—(a) Amplitude histogram rectangle and (b) the neural network necessary to model it.

neuron has a constant activation value of + 0.5 and is connected to all neurons in the succeeding layer (Dayhoff, 1990). The biases, like the interconnection weights, are learned during backpropagation. Thus, each forward pass through the hidden and output layer neurons implements the following activation equations (ANSim, 1988):

$$NET_i = \theta_i + \Sigma_j w_{ij} OUT_j \quad (4)$$

and

$$OUT_i = [1/(1 + e^{-NET_i})] - 0.5 \quad (5)$$

where θ_i is the bias for neuron i, and w_{ij} is the interconnection weight to neuron i from neuron j.

The bias neuron provides a constant threshold term θ_i in the weighted sum of the neurons in the succeeding layer which translates their sigmoid functions to the left or right depending upon its sign (Figure 7). This bias term results in an improvement on the convergence properties of the network during the training phase by keeping the sigmoids operating at their midrange values.

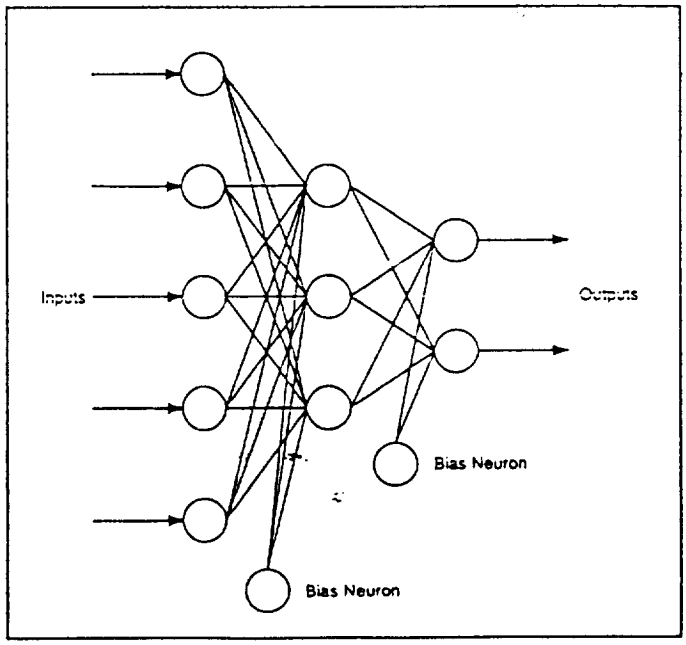

Figure 6—A typical three-layer network with bias neurons.

Biases and weight adjustments in the various layers are calculated using the generalized delta rule. This is a steepest descent method of computing the interconnection weights that minimizes the total squared output error over a set of training vectors (pairs). Each pass through the training set is called a cycle. After each training cycle, t, the following equation is used to calculate the total normalized root mean square (RMS) error, δ_t, for output neuron i:

$$\delta_t = \{[\Sigma_p \Sigma_i (TARGET_i - OUT_i)^2]/PI\}^{1/2} \quad (6)$$

Here, p is the training pair or pattern, P is the total number of training pairs or patterns, i is the output neuron, I is the total number of output neurons, and $TARGET_i$ = target output for neuron i.

The weight matrix changes are then backpropagated through each layer j within the network using the equation

$$w_{ij}(t+1) = \eta(\delta_i OUT_j) + a\, w_{ij}(t) \quad (7)$$

where η is the learning rate, a is the momentum, $\delta_i OUT_j$ is the current weight change, and $w_{ij}(t)$ is the previous weight change.

In theory, gradient descent is guaranteed only if infinitesimal changes are made to the weights. Because this would make the training process unacceptably long, a settable learning rate, η, is introduced. The goal is to set the learning rate as high as possible without causing the RMS error to oscillate significantly. This term is typically set between 0.01 and 1.0, depending upon the difficulty of the problem. The momentum term, a, is used to increase the learning rate without making the RMS error oscillate. The momentum determines what portion of the previous weight changes will be added to the current weight changes. This term is usually set to 0.9. In summary, by applying the generalized delta rule for backpropagation training, a multilayer neural network can learn to develop whatever features are necessary to perform the desired mapping from the input pattern to the target output.

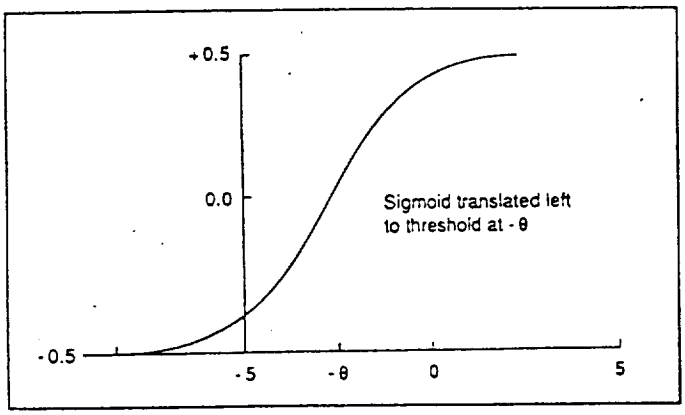

Figure 7—Sigmoid translation provided by threshold term θ_i

EXPERIMENTAL PROCEDURE

The eleven 5/16 by 1 by 12 in. (0.79 by 2.54 by30.48 cm) tensile test specimens were cut from butt welded sheets. Both sheets were made of 2195-T87 aluminum–lithium with a 2319 filler. In each case the weld was in the center of the specimen and perpendicular to the direction of pull.

A 10 kip (45360 kg)/min linear load ramp was generated by a computer-controlled Tinius Olsen tensile test machine. The load cell output ranged from 0.00 to 1.00 V (0.00 to 36.3 kips [16465.68 kg]). A Physical Acoustics Corporation (PAC) 3000/3004 acoustic emission analyzer and R15I piezoelectric sensor (with integral preamplifier) were used to collect the AE data. The AE sensor was taped to the specimen next to the weld and acoustically coupled using Sonotrace 40 ultrasonic couplant. The PAC 3000/3004 threshold was set at 0.3 V with a total system gain of 81 dB. This high system gain and low threshold were necessary to sense the predominantly ductile failure mechanisms inherent in the aluminum–lithium alloy.

In order to develop the technique, all eleven specimens were taken to failure with the AE sensor attached. These data were to be used to train the neural network to predict ultimate strengths from the AE data collected up to 25% of the expected ultimate strength, which would then become the proof load. The value for the expected failure strength was obtained by taking the average of the ultimate strengths for the training set. Once the network had been trained, the procedure would be to remove the sensor after the applying the proof load, then have the network make its ultimate strength prediction from the AE data taken up to that point.

DATA INPUT AND NETWORK ARCHITECTURE

The objective of this work was to predict the ultimate strength of a weld specimen from its AE amplitude data at proof loads well below yield, such that no macroscopic damage is done to the specimen. On viewing the amplitude distributions for all the weld specimens, it was found that the AE events having amplitudes greater than 50 dB were all associated with ultimate specimen failure (Figure 1). Such events only occur at *high* loads and therefore are not appropriate input for the prediction of ultimate strengths from the AE data taken at *low* loads. Consequently, only the event data in the amplitude range from 1 to 50 dB were input to the network.

In this case it was desired to map the extremely nonlinear curve $E(A)$ produced by the fifty input amplitude histogram into a single ultimate strength output, S_u. Given the appropriate number of neurons in the hidden layer, according to Kolmogorov's theorem (Caudill, 1988), a three-layer network exists that can perform this mapping exactly. For the problem at hand, the input dimension was $m = 50$, and the output dimension was $n = 1$; accordingly, a hidden layer of $2m+1 = 101$ artificial neurons would be required to produce an exact mapping. Unfortunately, an exact mapping for a given amplitude distribution does not guarantee a good prediction capability for other amplitude distributions.

Good prediction capability is obtained when the difference between the estimated amplitude distribution, $e(w_{ij},A)$, generated by a multilayer network with sigmoid activated neurons, and the actual distribution, $e(A)$, is minimized (Zurada, 1992). This error minimization is accomplished by making adjustments to the interconnection weights w_{ij} during supervised training using several representative input-output mappings or training pairs. Thus, an exact mapping is not desired—rather, a weighted approximation that minimizes the error over all the training pairs.

Since the desired mapping was going to be approximate anyway, it was decided to simplify the problem further by introducing a second approximation. Grouping the amplitudes into the previously discussed failure mechanism bands, the size of the hidden layer, and hence, the training time, was reduced considerably. Given that there were four failure mechanisms within the range of 1-50 dB (Figure 1), a reasonable guess for the reduced dimensionality of the problem was $m = 4$; whereupon, the number of neurons in the hidden layer necessary to exactly map the four humps became $2m+1 = 9$, which agreed quite well with the two neurons (perceptrons) per hump rule suggested previously. The sigmoid-generated humps shown in Figure 8 represent an approximation to the normally distributed humps of Figure 1.

Prior to training the network, the interconnection weights were initialized to small random numbers between -0.5 and +0.5, and the amplitude and ultimate strength data were normalized to fit into the same range (Lawrence, 1991). Designating the total number of acoustic emission events in the amplitude distribution up to the proof load as E_{max}, the normalized events at any given amplitude, $NE(A)$, were obtained from the equation

$$NE(A) = [E(A)/E_{max}] - 0.5 \quad (8)$$

where $E(A)$ was the number of AE events as a function of amplitude, A, from the amplitude distribution. The actual ultimate strengths, S_u, were normalized similarly:

$$NS_u = \{[S_u - (S_u)_l]/[(S_u)_u - (S_u)_l]\} - 0.5 \quad (9)$$

with NS_u the normalized ultimate strength, $(S_u)_l$ the lower range of

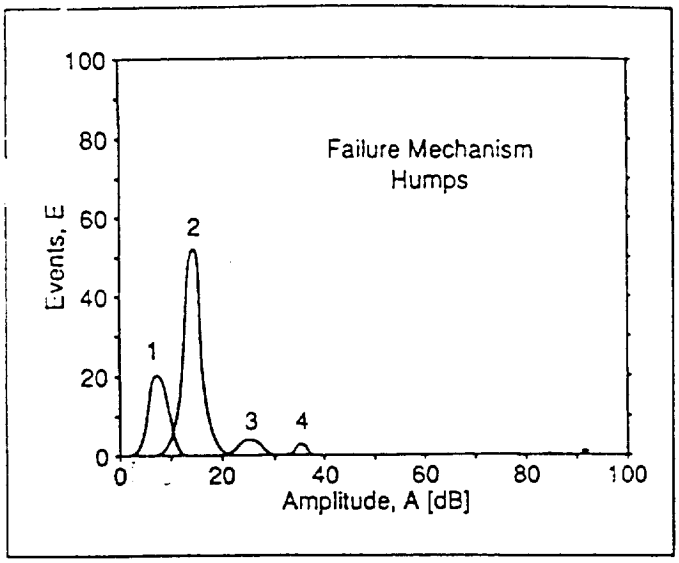

Figure 8—Sigmoid-generated failure mechanism humps.

the expected ultimate strengths, and $(S_u)_u$ the upper range of the expected ultimate strengths.

Here E_{max} was chosen to be 250 (slightly greater than the maximum number of events in any one of the eleven AE data sets), while $(S_u)_l$ was set at 45 ksi (0.310 kPa), and $(S_u)_u$ was set to 55 ksi (0.37 kPa). All of the above normalizations were effected to facilitate network training.

As was mentioned previously, several training pairs (specimens) were needed to train the network. It was also necessary to have sufficient variety in the training inputs such that the network would be able to make valid generalizations for unfamiliar cases—a good distribution of possible inputs and outputs, plus any border cases (Lawrence, 1991). Therefore, the five specimens chosen for the training set included the specimens with the highest ultimate strength, the lowest ultimate strength, and three intermediate values: 01-5, 01-8, 01-12, 01-13, and 01-14.

Some general rules apply when developing the network architecture for optimum performance (Bailey and Thompson, 1990). To improve accuracy on the training set, increase the size of the hidden layer(s). Alternately, to improve generalization capabilities and thus improve performance on new cases, reduce the size of the hidden layer(s). The optimal size for the hidden layer(s) is a balance between the objectives of accuracy and generalization for each application.

Table 1 Summary of the Neural Network Training

Network Name	Percentage Load Data	Training Cycles	RMS Training Error
BP_A_05.NET	100%	733	5%
BP_A_03.NET	100%	862	3%
BP_A_01.NET	100%	1,019	1%
BP_B_05.NET	50%	1,096	5%
BP_B_03.NET	50%	1,384	3%
BP_B_01.NET	50%	1,666	1%
BP_C_05.NET	25%	914	5%
BP_C_03.NET	25%	1,249	3%
BP_C_01.NET	25%	1,613	1%

RESULTS

The network architecture was optimized through trial and error. This resulted in an input layer of fifty neurons for the AE amplitude data, one hidden layer containing eight neurons for failure mechanism mapping, and an output layer comprised of a single neuron for ultimate strength. All the neurons were fully interconnected, making a total of 400 interconnection weights between the input and the hidden layer, S between the hidden layer and the output, plus 9 biases.

A summary of the neural network training is provided in Table 1. Altogether, nine networks were trained using the normalized amplitude data and the normalized ultimate strengths from the five specimen training set. In each case the learning rate was set to 0.2 and the momentum to 0.9. Three networks were trained using 100 percent of the AE amplitude data from load inception to specimen failure, one to a 5 percent RMS training error, one to a 3 percent error, and one to a 1 percent error. This procedure was then repeated for three networks using the AE data up to 50 percent of the expected failure load and for three using the data up to 25 percent of the expected failure load.

Because the ultimate strength data were normalized prior to input, the output prediction values from the neural network were also in a normalized format. As such, they had to be denormalized before any comparisons could be made. This was accomplished by inverting Equation 9:

$$(10) \qquad (S_u)_{pred} = (S_u)_l + [(S_u)_u - (S_u)_l][(NS_u)_{pred} + 0.5]$$

with the *pred* subscript denoting the predicted value.

Table 2 presents a summary of the actual versus predicted ultimate strengths and the associated errors for the three networks that were trained to a 3 percent RMS training error. (The 3 percent RMS training error seemed to optimize the prediction capability.) The AE data from all eleven specimens were applied to these three networks. This included the five specimens used as the training set and the six specimens from the test set. Note that the prediction errors on the five training set specimens were very small, as expected, while the prediction errors on the six test set specimens were of the same order of magnitude but slightly larger. The worst case error for the 25 percent load data was +2.6 percent for specimen 01-15.

Because the 25 percent load data contained the least amount of AE data, they were expected to yield the largest error, with the 50 percent data having the next largest error, and the 100 percent data having little or no error. This, however, was not found to be the case. Instead, the resulting errors were approximately the same for all three data sets.

Acoustic emission due to gripping noise was experienced for the first few hundred pounds of load before each specimen became seated in the test machine grips. The amount of AE activity associated with grip slip varied from test to test. While it was anticipated that this extraneous data might prevent accurate predictions, the neural networks were able to account for this effect and accurately predict ultimate strengths without removing it from the data set.

A few suggestions may be utilized for improving the prediction accuracy: (1) increase the accuracy of the input load data; (2) increase the number of specimens in the training set; and/or (3) add another AE parameter such as signal duration to allow better discrimination (Hill and Ely, 1992) between the various failure mechanisms. The other option is to employ probabilistic neural networks, or PNNs (Specht, 1990; Song and Schmerr, 1992). This would eliminate the need for a larger training set, because a good statistical sampling is all that is required, and it would speed up the training process, since only a single forward pass through the network is required. Also, because their activation functions are normal distribuations, PNNs might provide a more accurate fit to the normally distributed failure mechanism humps.

Besides accuracy, the other area of concern was that all of the welds tested here were essentially *good* welds. While porosity was observed in some of the specimens (01-5, 01-7, and 01-12), it was not enough to significantly affect their ultimate strengths. Moreover, there were no cracks nor any inclusions, and no areas of lack of

Table 2 Summary of the Actual vs. Predicted Ultimate Strengths of the Aluminum–Lithium Weld Specimens

Specimen	Actual Ult Str (ksi)	100% Load Data		50% Load Data		25% Load Data	
		Predicted Ult Str [ksi]*	% Error	Predicted Ult Str [ksi]*	% Error	Predicted Ult Str [ksi]	% Error
01–5+	51.5	51.0	–0.97	51.0	–0.97	51.0	–0.97
01–6	51.4	50.1	–2.53	50.0	–2.72	50.6	–1.56
01–7	51.2	50.0	–2.34	49.9	–2.54	49.9	–2.54
01–8+	51.0	50.9	–0.20	50.9	–0.20	51.0	0.00
01–9	50.8	50.6	–0.39	50.4	–0.79	50.3	–0.98
01–10	50.8	50.3	–0.98	50.3	–0.98	50.3	–0.98
01–11	50.6	50.1	–0.99	50.3	–0.59	50.4	–0.39
01–12+	49.9	50.0	0.20	50.0	0.20	50.0	0.20
01–13+	49.1	49.5	0.82	49.5	0.82	49.5	0.82
01–14+	50.4	50.5	0.20	50.5	0.20	50.4	0.00
01–15	49.5	50.6	2.22	50.3	1.62	50.8	2.63

\+ Training set * (Note: ksi units x 0.006895 = kPa)

penetration or lack of fusion. What is needed for future testing is some truly defective weld specimens. Training on both good and bad samples would then allow the network to predict the effect of defects on the ultimate strength of aluminum–lithium welds.

If a quantitative measure of structural integrity were needed, this technique could be extended to predicting the ultimate in-service strength (burst pressure) for the external tank itself. Using a backpropagation network, at least three external tanks would have to be hydroproofed to failure, two of which would contain known defects; five or six external tanks would be optimal for training purposes. By utilizing a probabilistic neural network, the number of full-scale tanks taken to failure could probably be minimized to three. Once trained, the neural network would be able to predict burst pressures in future external tanks from the AE data taken at hydroproof pressures well below yield (Hill, 1992). The obvious drawback to this scheme is the prohibitive cost of taking three external tanks to failure.

Since verification, not quantification, of structural integrity is normally the goal, a more cost-effective approach would be to use AE to monitor flaw growth activity during hydroproof (ASME, 1988; ASTM, 1987). Since growing flaws always emit and their acoustic signatures are distinctly different from other mechanisms and very locatable, radiography could be applied to *acoustically active* flaw growth areas only. This would provide a means of reducing the 100 percent x-ray inspection requirement currently imposed on the external tank welds (Nunes et al., 1984). Implementing such a procedure on the external tank would provide tremendous cost savings while maintaining the 100 percent inspection requirement for man-rated vehicles.

CONCLUSIONS

Ultimate strengths can be predicted in aluminum–lithium welds using AE amplitude data taken at loads up to 25 percent of the expected ultimate strength. This prediction was accomplished through the use of a fully interconnected backpropagation neural network with a single hidden layer. The network automatically accounted for the AE activity associated with grip slip (through the interconnection weights) without having to remove this extraneous data *a priori* from the data set. It also seemed to adjust for the overlap in the failure mechanism amplitudes. All of this was accomplished with a relatively small training set of only five specimens.

The fact that the prediction errors were essentially equal for the networks trained on the AE data set taken up to the ultimate load (100 percent load data), up to 50 percent of the ultimate load (50 percent load data), and up to 25 percent of the ultimate load (25 percent load data) meant that the same basic ultimate strength information was inherent in all three data sets. Thus, whatever AE parameters were keying the network prediction of ultimate strength were independent of any reduction in the AE data sets. This suggests the possibility of obtaining accurate ultimate strength predictions from the AE data at proof loads even lower than 25 percent of the expected ultimate load.

Finally, the +2.6 percent worst case ultimate strength prediction accuracy at 25 percent load was very close to the ±1.7 percent (± 0.005 V) accuracy of the input load data. Since the network prediction accuracy cannot exceed the accuracy of the input data, the network trained down to a 1 percent RMS error had larger prediction errors than either the networks trained to a 3 percent or a 5 percent error. An increase in accuracy of the input load data from three to four significant figures may well improve the predictions to within ±1 percent (Kalloo, 1988). The prediction accuracy of the networks was probably also constrained by the limited size of the training set, only five samples (as opposed to eleven for Kalloo's work).

Acknowledgments

This research was performed while on sabbatical leave at the NASA Marshall Space Flight Center under the auspices of the NASA/JOVE program, a jointly funded venture between Embry-Riddle Aeronautical University and NASA. Michael Suits ([205]) 544-8336) from the Non-Destructive Evaluation Branch of the Materials and Processes Laboratory served as the NASA project monitor, while the weld specimens were provided by Carolyn K. Russell ([205] 544-2705), Deputy Chief of the Metals Processes Branch.

References

ANSim User Manual, Scientific Applications International Corporation, San Diego, CA, 1988, pp 4-13 through 4-18.

ASME Boiler and Pressure Vessel Code, Article 12, Subsection A, Section V, "Acoustic Emission Examination of Metallic Vessels During Pressure Testing," American Society of Mechanical Engineers, New York, NY, Dec. 1988, Addendum.

ASTM Standard E 1139, "Practice for Continuous Monitoring of Acoustic Emission from Metal Pressure Boundaries," *Annual Book of ASTM Standards*, American Society for Testing and Materials, Philadelphia, PA, 1987.

Bailey, D., and D. Thompson, "How to Develop Neural-Network Applications," *AI Expert*, June 1990, pp 38–47.

Caudill, M., "Neural Networks Primer: Part III," *AI Expert*, June 1988,

continued on page 1051

Hagemaier, D.J., "Douglas Process Standard DPS 4.704, Rev. AG," 1992.
Jones, T., et al, "Reference Standards and Artificial Discontinuity Indications," *Nondestructive Testing Handbook*, Vol. 6, *Magnetic Particle Testing*, Section 14, pp 337–348, 1989. ASNT, Columbus, OH.
MIL-STD-1949; Military Standard, Inspection Magnetic Particle.
Skeie, K., and D. Hagemaier, "Quantifying Magnetic Particle Inspection," *Materials Evaluation*, Vol. 46, No. 6, May 1988, pp 779–785.
Swartzendruber, L., and R. Gaydos, "Progress on New Ring Standard," AMS Committee K, Progress Report, Jan. 1990.
Swartzendruber, L., "Aerospace Material Standard-Magnetic Particle Test Ring," Jan. 1991, and Revision 1, Mar. 1991.

Author

Donald J. Hagemaier is a staff manager and MDC Fellow at Douglas Aircraft Company in Long Beach, California. He has lectured extensively on aerospace NDE for the past 40 years and has published over 85 technical articles. He is an ASNT-certified Level III in six methods.

An ASNT Fellow since 1973, Hagemaier received ASNT's Achievement Award in 1972, ASNT's Lester Honor Award in 1984, and ASNT's Gold Medal Award in 1991. He received the Italian SNT Honorary Lecture Award in 1984, and was awarded the IAE Fellow and Outstanding Engineering Merit Award in 1992 upon nomination by SAE. Hagemaier received an AS in physics from Pierce Junior College, Woodland Hills, California, and majored in aeronautical engineering at Northrop Aeronautical Institute, Hawthorne, California. He is a registered professional quality engineer with the State of California.

---

continued from page 1045

pp 53–59.
Dayhoff, J.E., *Neural Network Architectures: An Introduction*, Van Nostrand Reinhold, New York, NY, 1990, pp 65–66.
Hill, E.v.K., "Predicting Burst Pressures in Filament-Wound Composite Pressure Vessels by Using Acoustic Emission Data," *Materials Evaluation*, Vol. 50, No. 12, 1992, pp 1439–1445.
Hill, E.v.K., and T.M. Ely, "Characterization of Failure Mechanisms in Graphite/Epoxy Tensile Test Specimens Using Acoustic Emission Data," *Fourth International Symposium on Acoustic Emission from Composite Materials*, American Society for Nondestructive Testing, Columbus, OH, 1992, pp 87–199.
Hill, E.v.K., and G.L. Knotts, "Predicting Ultimate Strengths of Aluminum-Lithium (Al-Li) Welds Using Acoustic Emission," *ASNT 1993 Spring Conference*, American Society for Nondestructive Testing, Columbus, OH, 1993, pp 81–83.
Kalloo, F.R., "Predicting Burst Pressures in Filament Wound Composite Pressure Vessels Using Acoustic Emission Data," MS Thesis, Embry-Riddle Aeronautical University, Daytona Beach, FL, 1988.
Kouvarakos, M., "Isolating Failure Mechanisms in a Fiberglass/Epoxy Tensile Test Specimen Using Acoustic Emission Signal Parameters," MS Thesis, Embry-Riddle Aeronautical University, Daytona Beach, FL, 1992.
Lawrence, J., "Data Preparation for a Neural Network," *AI Expert*, Nov. 1991, pp 34–41.
McBride, S.L., J.W. MacLachlan, and B.P. Paradis, "Acoustic Emission and Inclusion Fracture in 7075 Aluminum Alloys," *Journal of Nondestructive Evaluation*, Vol. 2, No. 1, 1981, pp 35–41.
Miller, R.K., and P. McIntire, eds., *Nondestructive Testing Handbook*, 2nd ed., 1987, Vol. 5, Acoustic Emission Testing, American Society for Nondestructive Testing, Columbus, OH, pp 103–107.
Mitchell, J.R., "Testing for Flaws in Reinforced Plastics by Acoustic Emission," *Plastics Engineering*, Jan. 1984, pp 29–32.
Nunes, A.C., Jr., E.O. Bayless, Jr., C.S. Jones III, P.M. Munafo, A.P. Biddle, and W.A. Wilson, "Variable Polarity Plasma Arc Welding on the Space Shuttle External Tank," *Welding Journal*, Vol. 63, No. 9, 1984, pp 27–35.
Pollock, A.A., "Acoustic Emission Amplitude Distributions," *International Advances in Nondestructive Testing*, Vol. 7, 1981, pp 215–239.
Sachse, W., and I. Grabec, "Intelligent Processing of Acoustic Emission Signals," *Materials Evaluation*, Vol. 50, No. 7, 1992, pp 826–834.
Song, S.J., and L.W. Schmerr, "Ultrasonic Flaw Classification in Weldments Using Probabilistic Neural Networks," *Journal of Nondestructive Evaluation*, Vol. 11, No. 2, 1992, pp 69–77.
Specht, D.F., "Probabilistic Neural Networks," *Neural Networks*, Vol. 3, No. 1, pp 109–118.
Tennant-Smith, J., *BASIC Statistics*, Butterworth & Co. Ltd., London, UK, 1985, p 106.
Walker, J.L., "Ultimate Strength Prediction of ASTM D-3039 Tensile Specimens from Acoustic Emission Amplitude Data," Paper No. 92-0258, presented at the AIAA 30th Aerospace Sciences Meeting, Reno, NV, Jan. 5–8, 1992.
Wasserman, P.D., *Neural Computing: Theory and Practice*, Van Nostrand Reinhold, New York, NY, 1989, pp 15–16, 19.
Zurada, J.M., *Introduction to Artificial Neural Systems*, West Publishing Co., St. Paul, MN, 1992, pp 7–8, 37–42, 55–56, 196–201.

Authors

Eric v. K. Hill is a Professor of Aerospace Engineering at Embry-Riddle Aeronautical University. He received both his BS in aerospace engineering (1970) and his PhD in mechanical engineering (1980) from the University of Oklahoma. His research interests are centered around applications of acoustic emission nondestructive testing to engineering problems, an area in which he has been studying or working for the past seventeen years.

An Assistant Professor of Computer Science at the Lamar University, Peggy L. Israel specializes in artificial intelligence, neural networks, and optimization. She earned a BS in mathematics from the University of Southwest Louisiana (1971) and a PhD in Computer Science from Tulane University (1990). Her current research is focused in two areas: neural network models for associative memory, pattern recognition, and optimization; and hybrid neural network/symbolic systems.

Gregory L. Knotts received his BS in Electrical Engineering from Youngstown State University (1979). He is a consultant for Acoustic Emission Consultants while pursuing a MS in industrial and systems engineering at the University of Alabama in Huntsville. His most recent work has been in software development for computed tomography and neural network analysis of AE data.